

Fig. 2. (A) Schematic representation of the interconnection of s-shaped moieties vertically, along [101], and along [100]. In the x-direction connection is achieved through two Sb3-S5-Sb3 bridges, which form the stippled 4-ring. A linkage out of the plane of the drawing is made through the S2 atom, here represented as a circle. Representation (B) is a view at almost 90° to (A) and shows the connections Sb1-S2-Sb2 responsible for the channels in this direction.

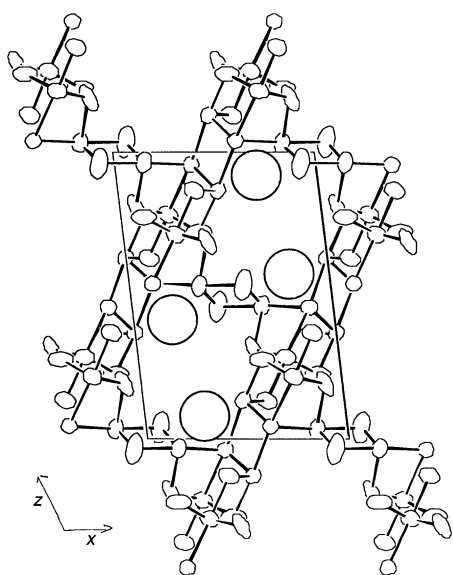


Fig. 3. The structure of SbS-Me₄N viewed down the crystallographic direction [010]. Circles represent the Me₄N⁺ molecules.

form the flat s-shaped structure shown in Fig. 1A, a collection of four fused 4-rings with composition [Sb₂S₂]²⁺. The s-shaped units are located close to the origin and body center of the unit cell (7) and are interconnected in two directions (Fig. 2). The buckled sheets of s-shaped units, close to the (010) plane, are connected together both by Sb3-S5-Sb3 bridges along the crystallographic direction [100] and by Sb1-S2-Sb2 bridges along [001]; compare Fig. 1 and Fig. 2A. These connections outline a channel along [010]. The second system of channels is formed along [100] by the interconnection of s-shaped units through Sb1-S2-Sb2 bridges, as shown in Fig. 2B.

The Me₄N molecules are contained within the channels as shown schematically in Fig. 3. Two orientations of the molecule randomly occupy the same site in the substructure. This feature, along with the disorder in one Sb and two S sites close to the Me₄N site, suggest that ordering of the template molecule within the channels may be responsible for the observed incommensurate superstructure.

It may be possible to connect the motif shown in Fig. 1 in a variety of ways; the obvious extensions of this work are the use of different templates and other lone-pair cations in attempts to produce new open frameworks. Along these lines, a number of

materials based on Sb₂S₃ have been synthesized and await characterization. The building principles for these and the other sulfide frameworks reported previously (5) also require elucidation, with a view toward enumerating possible sulfide networks and synthesizing materials with larger cavities and channels.

REFERENCES AND NOTES

1. Oft-cited general texts on the structures and properties of the zeolites and molecular sieves include D. W. Breck, *Zeolite Molecular Sieves* (Krieger, Malabar, FL, 1984); R. M. Barrer, *Zeolites and Clay Minerals as Sorbents and Molecular Sieves* (Academic Press, London, 1978); *Hydrothermal Chemistry of Zeolites* (Academic Press, London, 1982).
2. P. B. Weisz, *Mater. Res. Soc. Bull.* **14**, 54 (October 1989).
3. G. A. Ozin, A. Kuperman, A. Stein, *Angew. Chem. Int. Ed. Engl.* **28**, 359 (1989).
4. G. D. Stucky and J. E. Mac Dougall, *Science* **247**, 669 (1990).
5. R. L. Bedard, S. T. Wilson, L. D. Vail, J. M. Bennett, E. M. Flanigen, in *Zeolites: Facts, Figures and Future*, P. A. Jacobs and R. A. van Santen, Eds. (Elsevier, Amsterdam, 1989), pp. 375-387.
6. J. B. Parise, *Chem. Commun.* **1985**, 606 (1985).
7. Crystallographic data for Sb₃S₅-Me₄N: monoclinic, space group P2₁/n, a nonstandard setting of no. 14, a = 10.402(6), b = 9.447(2), c = 15.096(7) Å, β = 97.11(3)°, at 20°C and R factor (weighted R) = 0.060(5) (numbers in parentheses are standard errors in the last digit).
8. I am grateful to W. Marshall, R. Harlow, and J. C. Calabrese for their help and encouragement. I also acknowledge the generosity of the E. I. DuPont Company and the State of New York in providing a grant for my start-up at Stony Brook.

22 August 1990; accepted 7 November 1990

Local Structure and Chemical Shifts for Six-Coordinated Silicon in High-Pressure Mantle Phases

JONATHAN F. STEBBINS AND MASAMI KANZAKI*

Most of the earth's mantle is made up of high-pressure silicate minerals that contain octahedrally coordinated silicon (Si^{VI}), but many thermodynamically important details of cation site ordering remain unknown. Silicon-29 nuclear magnetic resonance (NMR) spectroscopy is potentially very useful for determining short-range structure. A systematic study of silicon-29 chemical shifts for Si^{VI} has revealed empirical correlations between shift and structure that are useful in understanding several new calcium silicates. The observed ordering state of a number of high-pressure magnesium silicates is consistent with the results of previous x-ray diffraction studies.

UNLIKE THE SILICATE MINERALS OF the crust and uppermost mantle of the earth, the silicates that form the bulk of the planet contain silicon coordinat-

ed by six (Si^{VI}) instead of by four O atoms (Si^{IV}). The basic structures of the compositional end-members of the most abundant of these high-pressure phases (for example, MgSiO₃ perovskite and garnet) are now known, but many details remain uncertain. In particular, solid solution and disorder of cations among multiple sites can have major effects on thermodynamic stability and thus on the range of pressures and temperatures over which the minerals form in the earth.

J. F. Stebbins, Department of Geology, Stanford University, Stanford, CA 94305.
M. Kanzaki, Department of Geology and C. M. Scarfe Laboratory for Experimental Petrology, University of Alberta, Edmonton, Canada AB T6G 2E3.

*Present address: Department of Chemistry, Arizona State University, Tempe, AZ 85281.

At high pressure and temperature, disorder is likely between Si^{VI} and Al^{VI} in phases such as garnet, ilmenite, and perovskite, and even disorder involving Mg^{VI} might occur. Similar structural questions arise for the titanate and aluminate analogs of these compounds, which are important in ceramic and electronic materials.

X-ray diffraction (XRD) remains the primary tool for determining the structures of minerals. However, diffraction generally gives only an average structure in a disordered material. In addition, the similarity of the atomic numbers of the abundant elements Mg, Al, and Si often means that their sites must be assigned indirectly by bond length rather than by x-ray scattering power. Other techniques must therefore supplement diffraction methods. One of the most useful of such techniques is magic-angle-spinning (MAS) NMR spectroscopy. Because of the relative simplicity of interpreting and quantifying spectra of dipolar nuclei, ^{29}Si MAS NMR spectroscopy has, for example, become the method of choice for evaluating short-range Al-Si ordering on tetrahedral sites in aluminosilicates (1). The method holds great promise for the determination of cation ordering in high-pressure Si^{VI} phases, as well as for investigating other details of their local structures and for characterizing small, polycrystalline experimental samples. Recently, the related approach of ^{27}Al MAS NMR has been used to study high-pressure garnets in the $\text{MgSiO}_3\text{-Mg}_3\text{Al}_2\text{Si}_3\text{O}_{12}$ system (2).

The relation between observed NMR isotropic chemical shifts (δ) and structure is difficult to predict from theory. The first step in the application of this technique thus must be to establish correlations between δ and known variations in structures. We therefore have carried out a systematic ^{29}Si NMR study of high-pressure silicates. These results are useful in predicting new, incompletely known phases, and they also test our general understanding of chemical shift systematics in a new class of structures.

The use of NMR to study minerals common in the earth at depths greater than about 150 km has been made possible only by the development of the multianvil high-pressure apparatus, coupled with improved spectroscopic methods. The materials described below were synthesized in a USSA-2000 split-sphere apparatus (C. M. Scarfe Laboratory for Experimental Petrology, University of Alberta) at pressures as high as 20 GPa and temperatures to 1800°C (Table 1). To improve NMR sensitivity with the resulting 2- to 10-mg samples (1/20 to 1/100 of the usual sample size for this type of spectroscopy), we used 95% $^{29}\text{SiO}_2$; 0.2% by weight Gd_2O_3 was added to de-

Table 1. Conditions and products of high-pressure experiments. Uncertainties in pressures are about ± 1 GPa for the MgSiO_3 experiments and about ± 0.5 GPa for the others. Primarily because of thermal gradients in capsules, uncertainties in temperatures are about $\pm 100^\circ\text{C}$ for pressures less than 15 GPa and about $\pm 200^\circ\text{C}$ at higher pressures. Phase names refer to structure type; see Table 2 for formulas. Phases X and Y are plotted in Fig. 2.

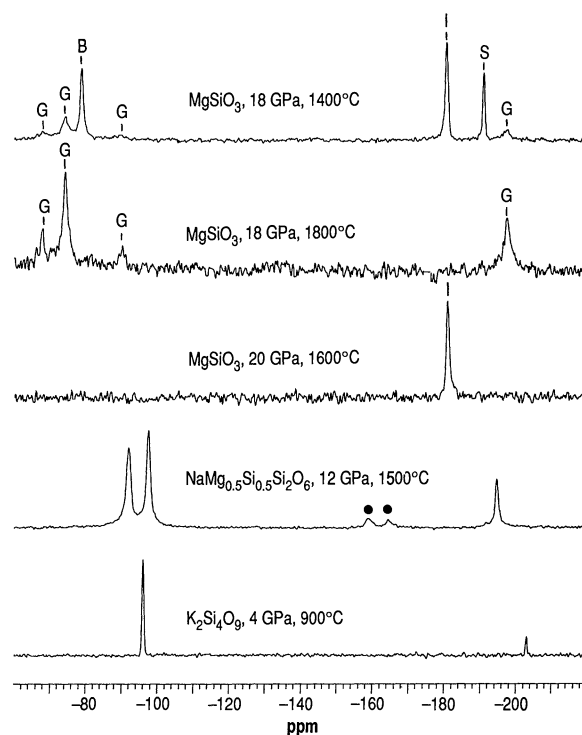
Composition	P (GPa)	T ($^\circ\text{C}$)	Products
MgSiO_3	18	1800	Garnet
MgSiO_3	20	1600	Ilmenite
MgSiO_3	18	1400	Garnet + ilmenite + stishovite + $\beta\text{-Mg}_2\text{SiO}_4$
CaSiO_3	12	1500	CaSi_2O_5 + larnite (= $\beta\text{-Ca}_2\text{SiO}_4$) + Y
CaSiO_3	15	1500	Amorphous + CaSi_2O_5 + X + Y + perovskite(?)
$\text{NaMg}_{0.5}\text{Si}_{0.5}\text{Si}_2\text{O}_6$	12	1500	Pyroxene
$\text{K}_2\text{Si}_4\text{O}_9$	4	900	Wadeite

crease spin-lattice relaxation times. Observed δ values and peak assignments (Figs. 1 and 2, Table 2) fell into the known ranges for Si^{IV} (-60 to -120 ppm) and for Si^{VI} (-179 to -220 ppm) in silicates, with one exception discussed below. Ilmenite-structured MgSiO_3 and $\text{NaMg}_{0.5}\text{Si}_{0.5}\text{Si}_2\text{O}_6$ pyroxene each showed only a single Si^{VI} peak. The presence of a single peak indicates that ordering of Si^{VI} and Mg^{VI} is complete, because (as for Si^{IV} in disordered aluminosilicates) variations among the first cation neighbors of Si^{VI} caused by Mg-Si disorder should result in multiple peaks. In the spectrum of the mixed-phase sample containing $\beta\text{-Mg}_2\text{SiO}_4$, the only feature not assignable to stishovite, garnet, or ilmenite is a single Si^{IV} peak. The lack of a Si^{VI} peak for $\beta\text{-Mg}_2\text{SiO}_4$ shows that all octahedral sites are occupied by Mg and that the cations are fully ordered. These results are fully consistent with published x-ray structure refine-

ments (3-5), as is the spectrum for the wadeite structure of $\text{K}_2\text{Si}_4\text{O}_9$ (6).

For the MgSiO_3 tetragonal garnet phase (Fig. 1), we observed at least three Si^{IV} peaks, which can be assigned to Si^{IV} with zero, two, and four Si^{VI} neighbors (and thus with four, two, and zero Mg^{VI} neighbors) with increasingly negative δ . These sites probably represent the three T sites of the x-ray structure (7), although the large separation in δ between the T3 (74 ppm) and T2 (90 ppm) peaks relative to that between the T3 and T1 (68 ppm) peaks is somewhat surprising. Simple considerations of the effects of neighboring cations suggest that the three peaks should be roughly evenly spaced, as is commonly observed for Si^{IV} sites in aluminosilicates that have increasing numbers of Al^{IV} neighbors. In the garnet structure, however, the presence of both octahedral and dodecahedral site neighbors complicates predictions of δ . In any case, the

Fig. 1. Silicon-29 MAS NMR spectra for various high-pressure phases. Measurements were made with a Varian VXR-400S NMR spectrometer with a 9.4-T magnet and a Doty Scientific, Inc., MAS probe. Chemical shifts are relative to tetramethylsilane. For most samples, 20,000 to 60,000 signal averages were collected with delay times of 1 to 10 s. A Gaussian smoothing function was applied that broadened lines by about 0.3 ppm. Spinning side bands are shown by solid circles. Peaks were assigned to the following phases (formulas in Table 2) on the basis of stoichiometry, NMR peak positions and areas, and x-ray diffraction data: G, garnet; B, $\beta\text{-Mg}_2\text{SiO}_4$; I, ilmenite; and S, stishovite. The $\text{NaMg}_{0.5}\text{Si}_{0.5}\text{Si}_2\text{O}_6$ sample crystallized to a single-phase pyroxene; the $\text{K}_2\text{Si}_4\text{O}_9$ formed the wadeite phase only.



reported space group of $I4_1/a$, which is the only subgroup of $Ia3d$ with three Si^{IV} sites (8), is strongly supported. Several smaller peaks may be unresolved in the broad envelope beneath the sharp spectral features. This pattern suggests that there is a small amount of octahedral Si-Mg disorder, con-

sistent with the x-ray data. The Si^{VI} peak for this sample is also relatively broad, as would be expected if the local Si^{VI} environments varied somewhat because of disorder. The configurational entropy S that results from this cation site mixing may have major effects on high-pressure phase equilibria. The

pressure-temperature (P - T) boundary curve between MgSiO_3 pyroxene and garnet has a negative slope ($dP/dT = \Delta S/\Delta V < 0$, where V is volume), and the curve between the garnet and higher pressure phases has a positive slope (9). This behavior is opposite to that observed for fully ordered analogs such as MnSiO_3 , CaGeO_3 , and CdGeO_3 (10).

For the CaO-SiO_2 system (11), our NMR and XRD data indicate that in a sample compressed at 12 GPa and 1500°C (Fig. 2, bottom) CaSiO_3 disproportionated into a mixture of $\beta\text{-Ca}_2\text{SiO}_4$ and a phase with a CaSi_2O_5 composition (12). The appearance of Si^{IV} and Si^{VI} peaks of roughly equal area for this phase suggests that its structure may be related to that of titanite ($\text{CaTi}^{\text{VI}}\text{-Si}^{\text{IV}}\text{O}_5$). A small peak at -150 ppm in this spectrum has the same δ as peaks attributed to five-coordinated Si in high-pressure alkali silicate glasses (13) but is much narrower. This shape suggests the presence of a small amount of a new crystalline phase of unknown structure containing this unusual Si coordination. The pairing of the -150 ppm peak with a Si^{IV} peak at -80 ppm of similar intensity indicates that the structure has a mixed coordination (phase Y).

At 16 GPa, in situ x-ray work in diamond-anvil pressure cells shows that CaSiO_3 transforms into a perovskite structure, which becomes amorphous on depressurization (14). The broad Si^{IV} NMR line for a sample

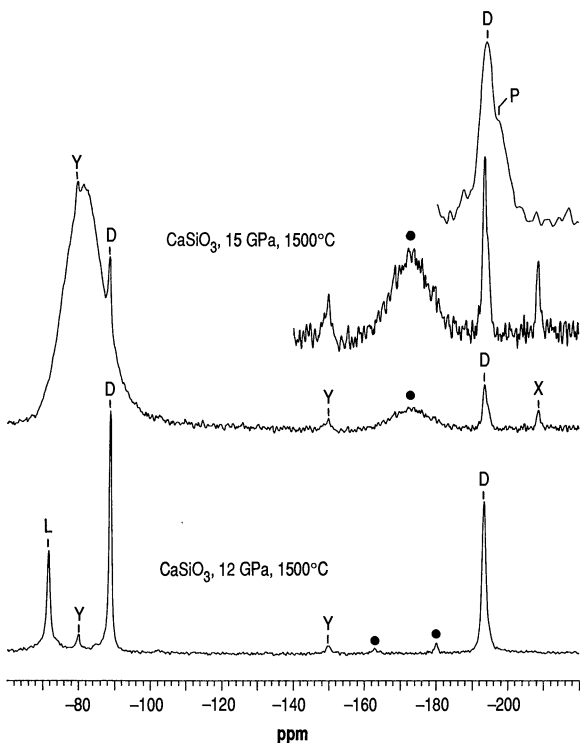


Fig. 2. Silicon-29 MAS NMR spectra for CaSiO_3 high-pressure phases. Experimental conditions were similar to those described in Fig. 1. The large, broad peak for the 15-GPa sample is caused by amorphous material produced on the depressurization of the perovskite phase. Marked peaks include: D, CaSi_2O_5 ; L, larnite ($\beta\text{-Ca}_2\text{SiO}_4$); Y, a new Ca silicate that apparently contains Si^{IV} and Si^{V} in roughly equal proportions; X, another new phase with high-coordinate Si; and P, CaSiO_3 perovskite. Two enlargements of portions of the spectrum for the 15-GPa sample are shown. The horizontal scale in the upper insert is expanded about the peaks near -194 ppm. In the lower insert, only the vertical scale is expanded.

Table 2. Measured and predicted negative ^{29}Si isotropic chemical shifts (in parts per million relative to tetramethylsilane) for crystalline oxides containing six- or five(?) -coordinated Si. Coordination numbers are shown

by Roman numerals. In the last column, the first number is the reference for structure, the second is for NMR data, and ts indicates this study.

Phase	Measured shift, Si^{IV}	$-d$	ΣEN	Measured shift, Si^{VI}	Predicted shift, Eq. 2	Predicted shift, Eq. 3	Reference
<i>Octahedral site data used in regressions</i>							
Thaumasite, H excluded		0.0378	21.64	179.6	178.7	183.0	(28, 29)
Thaumasite, H included*		0.2788	21.62	179.6	213.7	182.6	
$\text{MgSi}^{\text{VI}}\text{O}_3$ ilmenite		0.0526	21.62	181.0	180.9	182.7	(3), ts
Stishovite ($\text{Si}^{\text{VI}}\text{O}_2$)		0.1177	22.20	191.3	190.3	190.6	(30), ts
$\text{NaMg}_{0.5}\text{Si}^{\text{VI}}_{0.5}\text{Si}^{\text{IV}}_2\text{O}_6$ pyroxene	92.1, 97.6	0.1730	22.16	194.7	198.4	190.0	(4), ts
$\text{Mg}_4\text{Si}^{\text{VI}}\text{Si}^{\text{IV}}_3\text{O}_{12}$ garnet	68.0, 74.3, 90.3	0.1621	22.52	197.6	196.8	194.9	(7), ts
$\text{K}_2\text{Si}^{\text{VI}}\text{Si}^{\text{IV}}_3\text{O}_9$ wadeite	95.0	0.2219	23.33	203.1	205.5	205.8	(6), ts
$\text{Si}^{\text{VI}}_5\text{O}[\text{PO}_4]_6$, Si2 †		0.2565	24.06	214.0	210.5	215.5	(31, 25)
$\text{Si}^{\text{VI}}_5\text{O}[\text{PO}_4]_6$, Si1 †		0.2797	24.06	217.0	213.9	215.5	
<i>Data not included in regressions</i>							
$\text{MgSi}^{\text{VI}}\text{O}_3$ perovskite		0.1148	21.50	191.7	189.9	181.1	(32, 23)
$\text{CaSi}^{\text{VI}}\text{O}_3$ perovskite ‡		0.1367	21.82	194.5	193.7	185.4	(11), ts
$\text{CaSi}^{\text{IV}}\text{Si}^{\text{VI}}\text{O}_5$ §	88.9		22.69	193.4		197.2	(26), ts
Ca-silicate X				208.6			ts
Ca-silicate Y ($\text{Si}^{\text{V}}?$)				150.0			ts
$\text{Si}^{\text{VI}}\text{P}_2\text{O}_7$, Si1		0.2750	24.06	~220.	214.2	215.5	(24, 25)
$\text{Si}^{\text{VI}}\text{P}_2\text{O}_7$, Si2		0.2913	24.06	~220.	216.7		
$\text{Si}^{\text{VI}}\text{P}_2\text{O}_7$, Si3		0.3150	24.06	~220.	220.2		
$\text{Si}^{\text{VI}}\text{P}_2\text{O}_7$, Si4		0.3020	24.06	~220.	218.3		
$\text{Si}^{\text{VI}}\text{P}_2\text{O}_7$, Si5		0.2925	24.06	~220.	219.1		
$\text{Si}^{\text{VI}}\text{P}_2\text{O}_7$, Si6		0.2851	24.06	~220.	215.8		
$\beta\text{-Mg}_2\text{SiO}_4$	79.0						ts

*Thaumasite is $\text{Ca}_3[\text{Si}^{\text{VI}}(\text{OH})_6](\text{SO}_4)(\text{CO}_3) \cdot 15\text{H}_2\text{O}$. H^+ cations were included in the regression for Eq. 3, not for Eq. 2. †The average of the data for the two sites was used in the regression, as peak assignments are not known a priori. ‡The ideal cubic perovskite structure was assumed for the shift calculations, with $a = 0.3562$ nm. §Titanite ($\text{CaTi}^{\text{VI}}\text{Si}^{\text{IV}}\text{O}_5$) cation neighbor populations were assumed for the calculation.

that we synthesized at 15 GPa (Fig. 2, top) in the multianvil apparatus shows that most of the material is indeed amorphous. However, small, narrow peaks for crystalline phases are also evident. These include the Si^{IV}-Si^{VI} pair for the CaSi₂O₅ and the possible Si^{IV}-Si^V pair noted in the 12-GPa sample. Powder XRD data on similar samples of natural isotopic abundance show small amounts of quenched CaSiO₃ perovskite, which may be the source of the poorly resolved, small peak at -194.4 ppm (15). Another small Si^{VI} peak at -208.6 (phase X) indicates that a second new phase formed under these disequilibrium conditions. This value of δ is, intriguingly, the most negative shift observed for a P-free silicate.

The most important effects on δ for Si^{IV} in silicates are those of the number and field strength of the first-neighbor cations. Probably because of decreased paramagnetic deshielding (16), smaller, more highly charged cations cause a magnetically more shielded local environment and thus more negative δ values. This general pattern is also clear in the data for Si^{VI} (Table 2). When the first neighbor cation is P⁵⁺, the most extreme shifts are observed. Si^{VI} sites with Si^{IV} neighbors (wadeite, garnet, NaMg_{0.5}-Si_{0.5}Si₂O₆ pyroxene) are less shielded, followed by those with Si^{VI} neighbors (perovskite, stishovite, ilmenite), and finally by thaumasite with no Si neighbors at all.

Several more specific relations between δ and variables that described the local structure have been reported for Si^{IV} in silicates of widely varying structural class (17-19). Sheriff and Grundy (19) described an excellent linear relation between δ and a variable χ' (reabeled here as d) that was based on the effects of magnetic susceptibility anisotropy (MSA) on proton shifts in organic molecules (20). Their equation 2 includes a standard geometric term that is multiplied by a measure of the strength of the cation-O bond and that is summed over all first-neighbor cations X:

$$d = \sum_i s_i [(1 - \cos^2 \theta_i) / 3R_i^3] \quad (1)$$

Here s_i is the bond valence as defined by Brown and Altermatt (21), θ is the angle between the O-X vector and the vector from the central Si to the midpoint of the O-X bond, and R is the length of the latter vector. The geometric term is only a rough approximation to theory for substituent groups that are as close to the central Si as those considered here. Also, the bond-valence term only proxies for the MSA for each O-X bond, which is generally unknown in these materials. However, it does make sense that a more ionic bond (smaller bond valence) should have a smaller MSA, because the electron distribution is more

spherical. The sign of the bond-valence term implies that the major effect on shielding is that of the paramagnetic term, as in the model based on group electronegativity described below.

The original fit equation for Si^{IV} sites (19) poorly predicts observed Si^{VI} data (Fig. 3). However, an excellent independent relation is found between d and δ for Si^{VI} sites only (22), with

$$\delta = 145.4d - 173.2 \text{ (SD = 2.7 ppm)} \quad (2)$$

where SD is the standard deviation of the points about the line. For thaumasite, δ is poorly predicted if H⁺ ions in the structure are included, as was found for Si^{IV} sites (19). This problem suggests that proton mobility may somehow average the effects of this cation on δ , or that H⁺ sites are not accurately located. The predicted δ for MgSiO₃ perovskite agrees well with that observed (23). For the complex structure SiP₂O₇, which has six distinct Si^{VI} sites (24), a range of shifts from -214 to -220 ppm is predicted that sum to give a single broad peak, similar to that previously reported (25).

A second approach correlates δ with the sum of the group electronegativities (Σ EN) derived for each type of O-X bond (18). We have taken published results for O-Ca, O-Mg, and O-H bonds (18), assumed an average value of EN for O-Si^{IV} bonds of 4.00 and assumed that EN for O-K bonds is approximated by that for O-Na bonds, and have derived EN values for O-Si^{VI} bonds of 3.70 and for O-P bonds of 4.01 from the data set for octahedrally coordinated phases. We calculated Σ EN using equation 4 of Janes and Oldfield (18), treating all cations as nonframework species, and found a good relation between Σ EN and δ (Fig. 4):

$$\delta = -13.48 \Sigma \text{EN} + 108.7 \quad (3)$$

(SD = 3.1 ppm)

The prediction of this equation for MgSiO₃ perovskite is, however, relatively poor.

The chemical shifts for both Si^{IV} and Si^{VI} sites appear to fall on a single nonlinear curve if plotted against Σ EN (Fig. 4). This result supports the assumption that peaks near to -150 ppm are caused by Si^V sites. If, for example, there were sites in the Ca silicate phase Y that had five Si^{IV} and ten Ca cation neighbors (analogous to a garnet structure), then the calculated Σ EN and the observed δ fall just where expected between the data for Si^{IV} and Si^{VI}.

The structure of CaSiO₃ perovskite is not yet known in detail, but powder XRD data indicate that it has a cubic unit cell with $a = 0.3562$ nm (11). Taking the ideal perovskite structure as an approximation and using Eq.

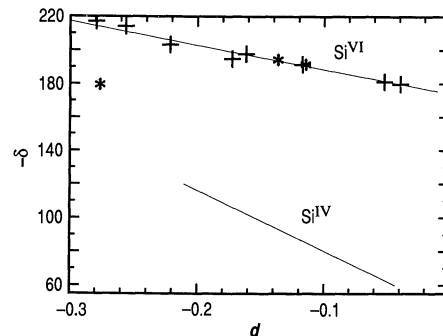


Fig. 3. Measured chemical shifts versus the variable d (Eq. 1) for octahedral Si sites in oxides, with the fit line of Eq. 2. Points marked by * were not used in this regression and include Ca and Mg perovskite. Two points are shown at -179.6 ppm for thaumasite: one lies on the fit line, the other, calculated including H⁺ ions, is the extreme outlier below the line. The lower line shows the fit to data for tetrahedral sites of equation 3 of Sheriff and Grundy (19).

2, we predict that $\delta = -193.6$, close to the peak at -194.4 ppm seen in the spectrum of the 15-GPa sample. Use of Eq. 3 does not require detailed structural information (and thus this approach is less precise) but yields a similar difference of 4.3 ppm between Mg and Ca perovskites. Assuming that the new CaSi₂O₅ phase has a titanite-like cation neighbor distribution (26) and using Eq. 3, we predict a shift within 4 ppm of that observed. Finally, both models suggest that peak X in the 15-GPa CaSiO₃ sample is caused by an unknown new structure with a large number of high-field strength cation neighbors such as Si^{IV} (27). If this is the case, an additional Si^{IV} peak must be obscured by the large peak for the amorphous material.

Both fitting procedures (Eqs. 2 and 3) were originally based only on data for Si^{IV}. Their reasonably good success for the rather different Si^{VI} structures suggests that both have real physical significance. Theoretical

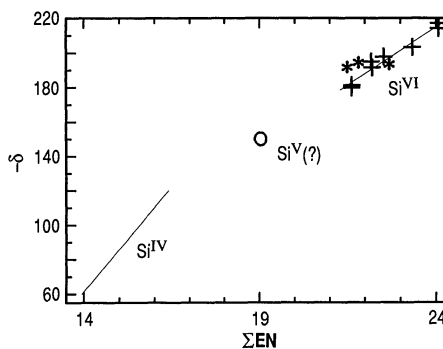


Fig. 4. Measured chemical shifts versus Σ EN for octahedral Si sites in oxides, with the fit line of Eq. 3. Three points not included in the regression are shown by *; these include Ca and Mg perovskite and CaSi₂O₅. Also shown is the fit line for tetrahedral sites from equation 1 of Janes and Oldfield (18). The open circle is the presumed Si^V site in Ca silicate phase Y, calculated for five Si^{IV} and ten Ca neighbors.

justifications for the two types of equation are related but somewhat different. However, the important point is that in crystal structures many different structural variables can be highly correlated, with none that by itself describes all magnetic interactions. More work on a wider range of compositions, and particularly single-crystal ^{29}Si NMR studies, is needed to understand such models completely.

31. H. Mayer, *Monatsh. Chem.* **105**, 46 (1974).
32. H. Horiuchi, E. Ito, D. J. Weidner, *Am. Mineral.* **72**, 357 (1987).
33. Supported under U.S. National Science Foundation grants EAR 85-53024 and EAR 89-05188 to J.F.S., and Natural Sciences and Engineering Research

Council of Canada grants SMI-105, CII0006947, and OGP0008394 to the late C. M. Scarfe. We thank X. Xue for help with data collection and the two anonymous reviewers for useful comments.

4 September 1990; accepted 24 October 1990

Arctic Lakes and Streams as Gas Conduits to the Atmosphere: Implications for Tundra Carbon Budgets

GEORGE W. KLING,* GEORGE W. KIPPHUT,† MICHAEL C. MILLER

Arctic tundra has large amounts of stored carbon and is thought to be a sink for atmospheric carbon dioxide (CO_2) (0.1 to 0.3 petagram of carbon per year) (1 petagram = 10^{15} grams). But this estimate of carbon balance is only for terrestrial ecosystems. Measurements of the partial pressure of CO_2 in 29 aquatic ecosystems across arctic Alaska showed that in most cases (27 of 29) CO_2 was released to the atmosphere. This CO_2 probably originates in terrestrial environments; erosion of particulate carbon plus ground-water transport of dissolved carbon from tundra contribute to the CO_2 flux from surface waters to the atmosphere. If this mechanism is typical of that of other tundra areas, then current estimates of the arctic terrestrial sink for atmospheric CO_2 may be 20 percent too high.

ARTIC ECOSYSTEMS ARE EXPECTED to be strongly affected by future climatic change (1–3), and, if these ecosystems either accumulate additional C or lose C to the atmosphere, they will be important to the global C budget (4–8). At present, tundra ecosystems appear to be small sinks for C; that is, the amount of C extracted from the atmosphere during photosynthesis is slightly more than that respired by plants and soils and lost to the atmosphere (7, 9). But there is evidence that additional C loss to and from aquatic ecosystems may also be significant. One type of loss, by erosion of peat into lakes and rivers, can be a substantial part of the long-term accumulation rate of terrestrial C (10, 11). There is also some indication that terrestrial C washed into lakes is respired and lost to the atmosphere as CO_2 (10, 12). It is not known how widespread these CO_2 losses from surface waters are, and thus to what extent tundra C budgets are affected. In this report, we describe measurements of CO_2 concentration and flux from 25 lakes and 4 rivers on the North Slope of Alaska. Our results suggest that the transport of dissolved C from terrestrial to aquatic environments is significant.

We sampled locations on the North Slope of arctic Alaska within several kilometers of

the oil pipeline and between the foothills of the Brooks Range and Prudhoe Bay on the Arctic Ocean (Table 1). Partial pressures of CO_2 (P_{CO_2}) were obtained by direct measurement or by calculation from data on pH, temperature, and concentrations of alkalinity or dissolved inorganic C (DIC) (13). The CO_2 flux was calculated from partial pressure differences between air and water and an estimated gas transfer coefficient, or measured directly at one site with a floating chamber (14). We used a gas transfer coefficient of 2.1 cm hour^{-1} for all sites; this value could be too small (15), and therefore our calculated CO_2 fluxes may well underestimate actual fluxes.

Although these lakes and rivers lie in varied terrain, we observed no systematic patterns of CO_2 flux with site location, lake area, or maximum depth. The average P_{CO_2} value for surface waters of all lakes was 1162 ± 134 parts per million by volume (ppmv) (± 1 SE), which is supersaturated by more than three times with respect to the atmosphere (Table 1). The flux of CO_2 from water to the atmosphere ranged from -5.5 to $59.8 \text{ mmol m}^{-2} \text{ day}^{-1}$ and averaged $20.9 \pm 3.3 \text{ mmol m}^{-2} \text{ day}^{-1}$ in the lakes and $7.1 \pm 3.0 \text{ mmol m}^{-2} \text{ day}^{-1}$ in the rivers.

Annual variations in CO_2 flux are small for lakes with a long run of data (Table 1). Multiyear trends in flux are absent, and much of the interannual variation is probably a result of the fact that sampling was done at different times of the year. In Toolik Lake, the highest CO_2 evasion rates occurred early in the season in most of the 9 years studied (Fig. 1). These high, early-

REFERENCES AND NOTES

1. G. Engelhardt and D. Michel, *High-Resolution Solid-State NMR of Silicates and Zeolites* (Wiley, New York, 1987).
2. P. McMillan et al., *Phys. Chem. Minerals* **16**, 428 (1989).
3. H. Horiuchi, M. Hirano, E. Ito, Y. Matsui, *Am. Mineral.* **67**, 788 (1982).
4. R. J. Angel et al., *Nature* **335**, 156 (1988).
5. H. Horiuchi and H. Sawamoto, *Am. Mineral.* **66**, 568 (1981).
6. D. K. Swanson and C. T. Prewitt, *ibid.* **68**, 581 (1983).
7. R. J. Angel et al., *ibid.* **74**, 509 (1989).
8. Y. Takeuchi, N. Haga, S. Umizu, G. Sato, *Z. Kristallogr.* **158**, 53 (1982).
9. D. C. Presnall and T. Gasparik, *Eos* **70**, 483 (1989).
10. A. Navrotsky, in *High-Pressure Research in Mineral Physics*, M. H. Manghnani and Y. Syono, Eds. (American Geophysical Union, Washington, DC, 1987).
11. M. Kanzaki, J. F. Stebbins, X. Xue, in preparation.
12. A phase of unknown structure, labeled ϵ , has been reported as a product of decomposition of CaSiO_3 [A. E. Ringwood and A. Major, *Earth Planet. Sci. Lett.* **2**, 106 (1967); H. Tamai and T. Yagi, *Phys. Earth Planet. Inter.* **54**, 370 (1989)]. Our results (11) indicate that this material was probably a mixture of a new phase of CaSi_2O_5 stoichiometry and $\beta\text{-Ca}_2\text{SiO}_4$.
13. J. F. Stebbins and P. McMillan, *Am. Mineral.* **74**, 965 (1989); X. Xue, J. F. Stebbins, M. Kanzaki, P. McMillan, B. Poe, *ibid.*, in press.
14. L. Liu and A. E. Ringwood, *Earth Planet. Sci. Lett.* **28**, 209 (1975).
15. The ^{29}Si -enriched CaSiO_3 sample probably had a slight excess of SiO_2 : the 15-GPa sample with natural isotopic abundance showed XRD peaks for perovskite only (11).
16. R. K. Harris, *Nuclear Magnetic Resonance Spectroscopy* (Pitman, London, 1983).
17. K. A. Smith, R. J. Kirkpatrick, E. Oldfield, D. M. Henderson, *Am. Mineral.* **68**, 1206 (1983).
18. N. Janes and E. Oldfield, *J. Am. Chem. Soc.* **107**, 6769 (1985).
19. B. L. Sheriff and H. D. Grundy, *Nature* **332**, 819 (1988).
20. H. M. McConnell, *J. Chem. Phys.* **27**, 226 (1957).
21. I. D. Brown and D. Altermatt, *Acta Crystallogr. Sect. B* **41**, 244 (1985).
22. All cations (except for the central Si) within 0.3 nm of each O ligand were included in the sums. Inclusion of a second shell of cations makes little difference in the value of d because of the R^3 term in the equation. Atomic positions were calculated with the program Atoms (Shape Software, Inc.).
23. R. J. Kirkpatrick, personal communication.
24. E. Tillmans, W. Gebert, W. H. Bauer, *J. Solid State Chem.* **7**, 69 (1973).
25. T. L. Weeding, B. H. W. S. deJong, W. S. Veeman, B. G. Aitken, *Nature* **318**, 353 (1985).
26. J. A. Speer and G. V. Gibbs, *Am. Mineral.* **61**, 238 (1976).
27. A second, rather speculative possibility is a Si site with more than six O neighbors.
28. R. A. Edge and H. F. W. Taylor, *Acta Crystallogr. Sect. B* **27**, 594 (1971).
29. A. Grimmer et al., *Z. Chem.* **20**, 453 (1980).
30. W. H. Bauer and A. A. Khan, *Acta Crystallogr. Sect. B* **27**, 2133 (1971).

G. W. Kling, The Ecosystems Center, Marine Biological Laboratory, Woods Hole, MA 02543.

G. W. Kipphut, Institute of Marine Science, University of Alaska Fairbanks, Fairbanks, AK 99775.

M. C. Miller, Department of Biological Sciences, University of Cincinnati, Cincinnati, OH 45221.

*To whom correspondence should be addressed.

†Present address: Center for Great Lakes Studies, University of Wisconsin, Milwaukee, WI 53204.